

## Supplementary material

### **Hierarchical CuO Octahedra Inherited from Copper Metal-Organic Frameworks: High-Rate and High-Capacity Lithium-Ion Storage Materials Stimulated by Pseudocapacitance**

*Xiaoshi Hu, Chao Li, Xiaobing Lou, Qi Yang\* and Bingwen Hu\**

State Key Laboratory of Precision Spectroscopy, Shanghai Key Laboratory of magnetic resonance, Institute of Functional Materials, School of Physics and Materials Science, East China Normal University, Shanghai 200062, PR China.

\*E-mail: qyang@lps.ecnu.edu.cn; bwhu@phy.ecnu.edu.cn.

## Contents

Figure S1. TG analysis of Cu-MOF.

Figure S2. TG curves of the CuO product.

Figure S3. High-magnification SEM (a) and TEM (b, c) images of HPCOs with different magnifications (as illustrated).

Figure S4. EDX analysis of HPCOs: (a) EDX spectra, (b) SEM images, (c) Cu, and (d) O elemental mapping images in the area (b).

Figure S5. PXRD patterns of the products formed in the NaOH solutions with various concentrations and reaction times.

Figure S6. SEM images of the products formed in the NaOH solutions with concentrations and reaction times of (a) 0.1 M, 3 d, and (b) 1 M, 2 h.

Figure S7. Coulombic efficiencies of HPCO electrode when cycling at 0.1 A g<sup>-1</sup>.

Figure S8. Electrochemical impedance plots (top, experiment dates: circles, and simulation results: solid lines) and equivalent circuit (bottom) of as-fabricated HPCO anodes.

Figure S9.  $lg i$  vs.  $lg v$  plots at different oxidation and reduction states.

Table S1. Comparison of specific capacities, rate performance and cycling stability of our work with reported Cu<sub>x</sub>O-based electrode materials for LIBs.

Table S2. The resistances determined by EIS with cycling for HPCO electrode. Values were calculated with the above equivalent circuit model in Figure S5 (bottom).

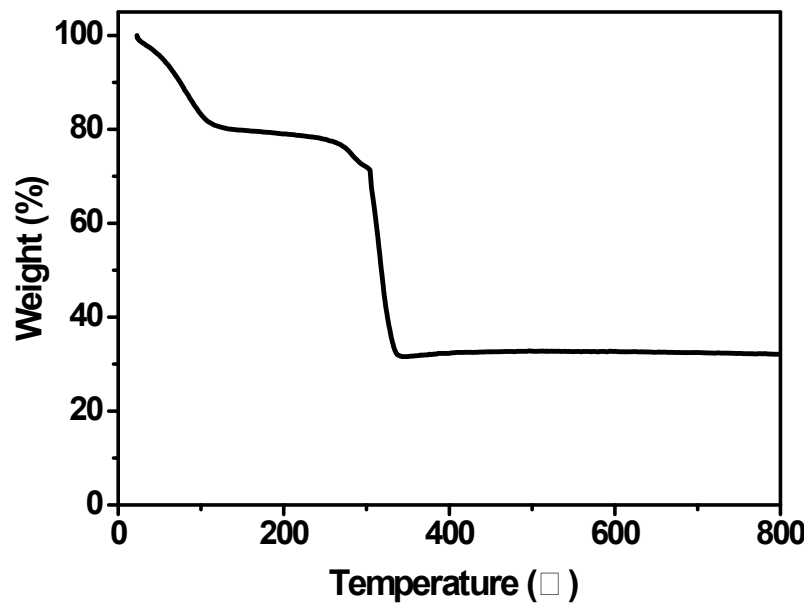


Figure S1. TG analysis of Cu-BTC MOF.

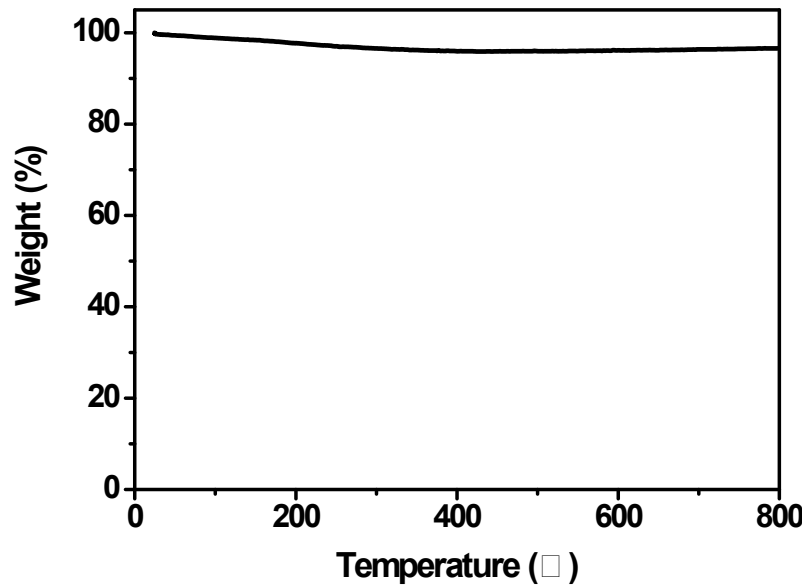


Figure S2. TG curves of the CuO product.

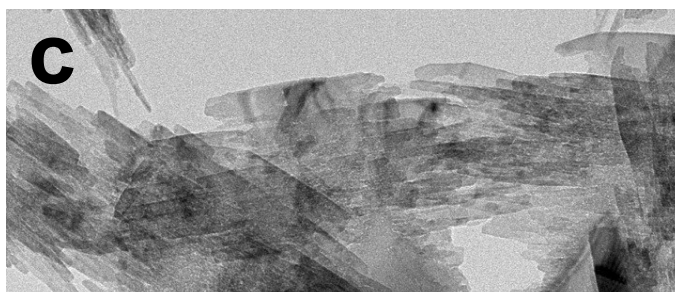
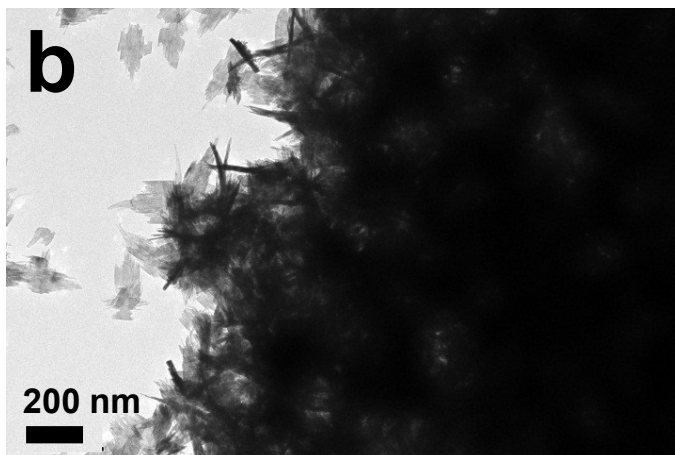
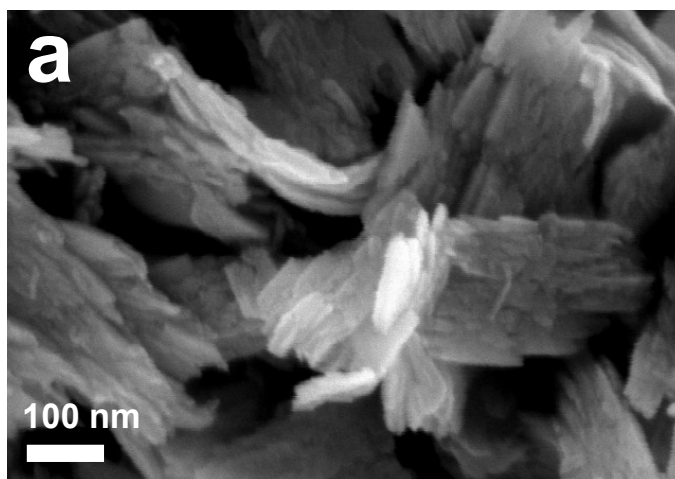


Figure S3. High-magnification SEM (a) and TEM (b, c) images of HPCOs with different magnifications (as illustrated).

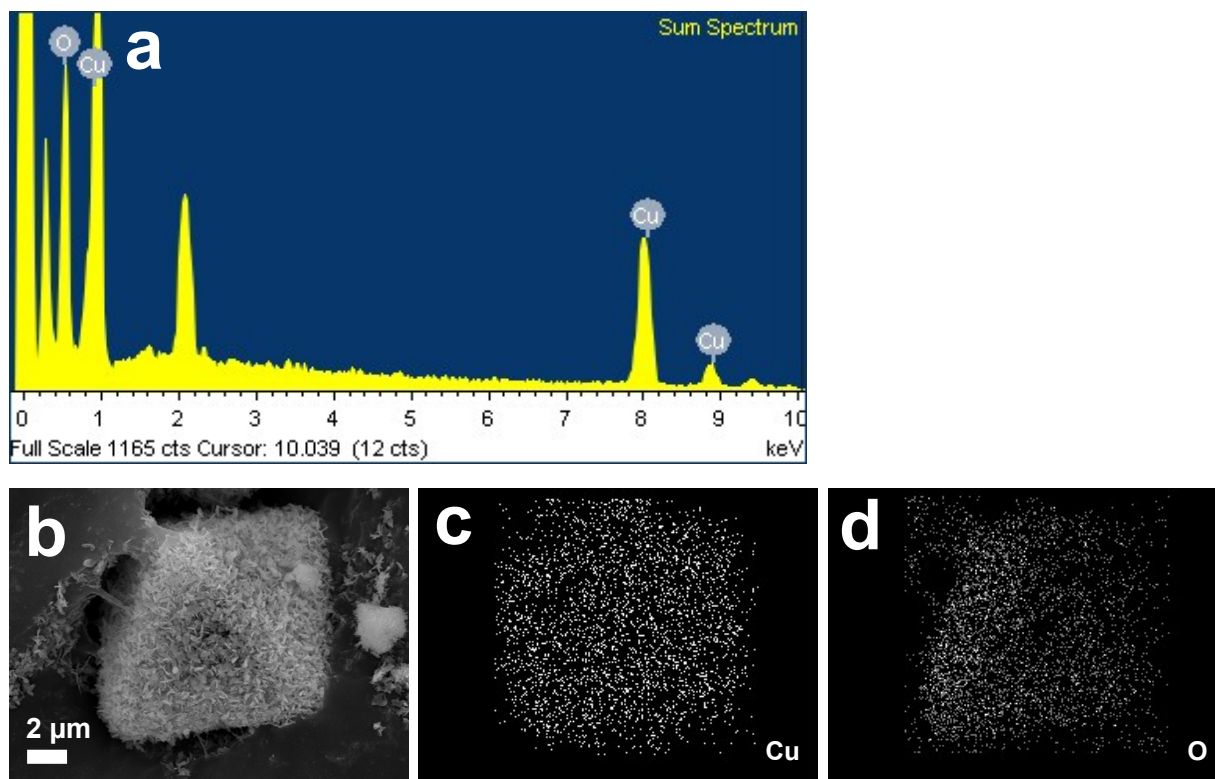


Figure S4. EDX analysis of HPCOs: (a) EDX spectra, (b) SEM images, (c) Cu, and (d) O elemental mapping images in the area (b).

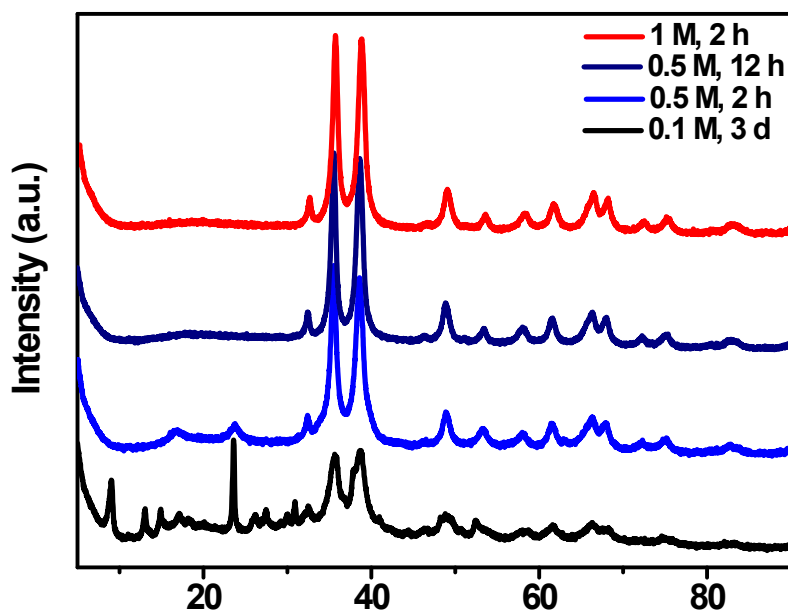


Figure S5. PXRD patterns of the products formed in the NaOH solutions with various concentrations and reaction times.

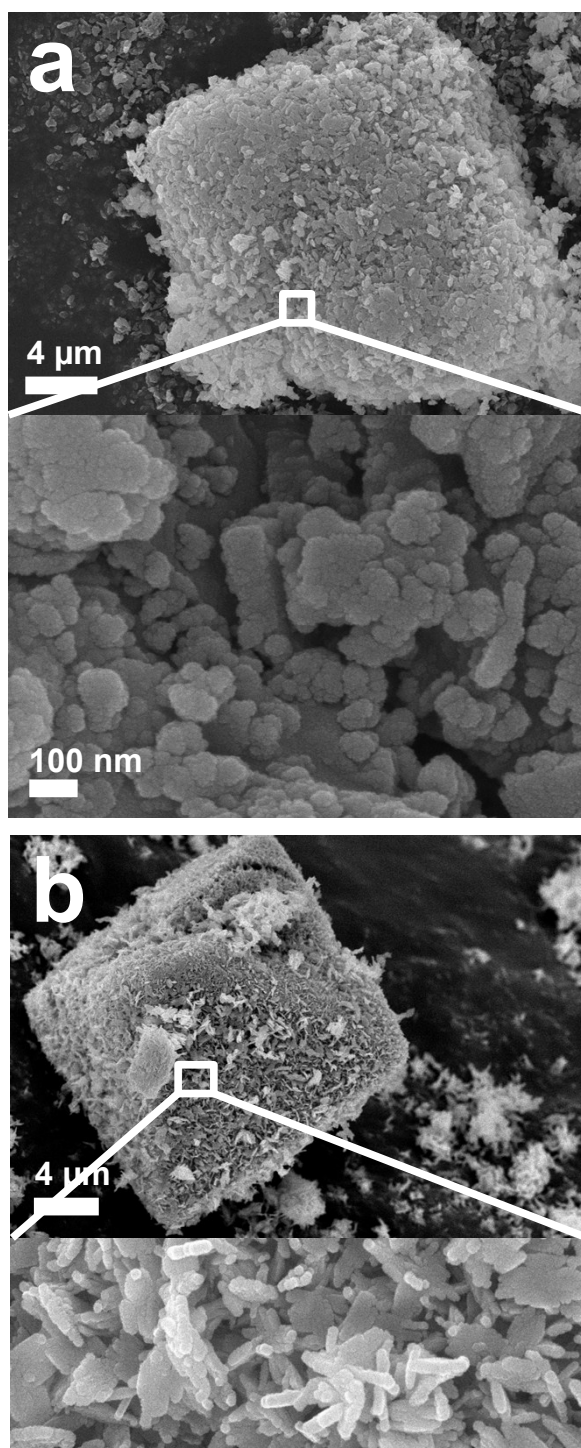


Figure S6. SEM images of the products formed in the NaOH solutions with concentrations and reaction times of (a) 0.1 M, 3 d, and (b) 1 M, 2 h.

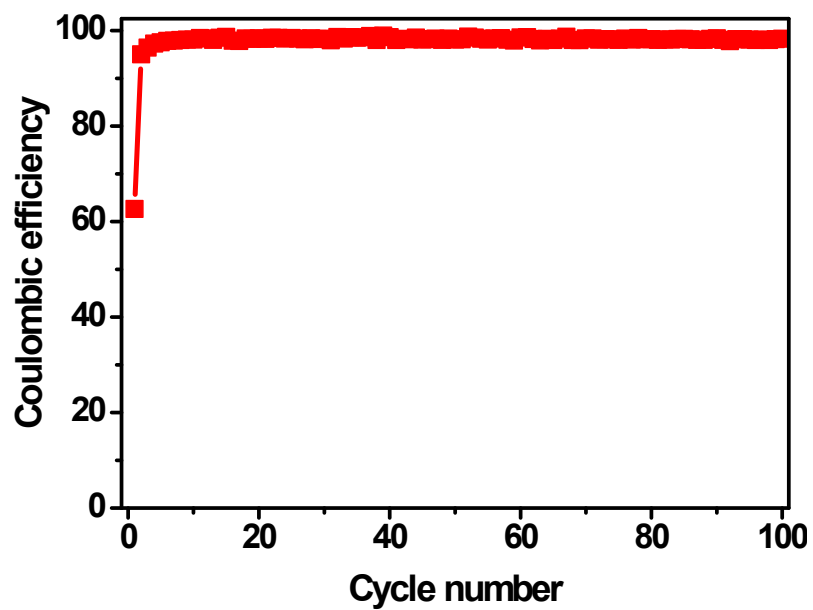


Figure S7. Coulombic efficiencies of HPCO electrode when cycling at  $0.1 \text{ A g}^{-1}$ .

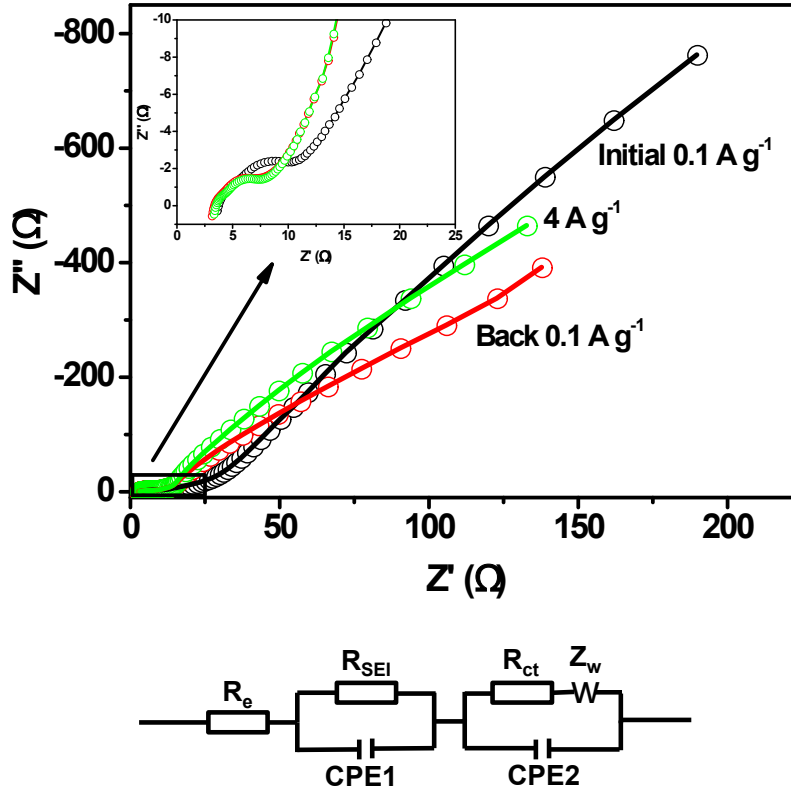


Figure S8. Electrochemical impedance plots (top, experiment dates: circles, and simulation results: solid lines) and equivalent circuit (bottom) of as-fabricated HPCO anodes. The plots are recorded during multiple-step galvanostatic tests after completing 10, 60 and 170 cycles, respectively. The features of the Nyquist plots (top) can be explained on the basis an equivalent circuit model, as indicated in bottom as follows: the intercept of the high-frequency semicircle on the  $Z'$  axis is the electrolyte resistance ( $R_e$ ), the high-frequency semicircle is an indication of the SEI layer resistance ( $R_{SEI}$ ) and capacitance (CPE1), the middle-frequency semicircle corresponds to charge transfer resistance ( $R_{ct}$ ) and the double-layer capacitance (CPE2), and the inclined line at low-frequency region represents the Warburg impedance ( $Z_w$ ) related to lithium diffusion in the solid.

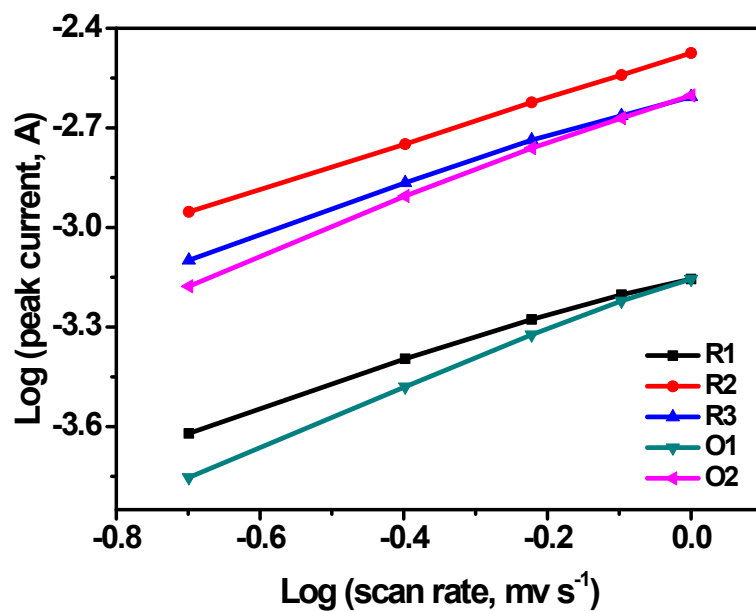


Figure S9.  $\lg i$  vs.  $\lg v$  plots at different oxidation and reduction states.

Table S1. Comparison of specific capacities, rate performance and cycling stability of our work with reported Cu<sub>x</sub>O-based electrode materials for LIBs.

Electrode materials		Current density (A g <sup>-1</sup> )	Cycle number	Specific capacity (mA h g <sup>-1</sup> )	Refs
MOF-room temperature transformation	HPCOs	0.1, 0.5, 2, 5	140, 200, 200, 400	1201, 1062, 615, 423	This work
MOF-calcination	pyramidal nanostructured CuO	0.1	40	484.2	29
	CuO/Cu <sub>2</sub> O hollow polyhedrons	0.25	250	740	31
	porous CuO hollow octahedra	0.1	100	470	30
	CuO/Cu <sub>2</sub> O-GPC	0.06	200	887.3	6
	hollow porous CuO/C microcubes	0.1	200	510.5	33
	multi-yolk-shell CuO@C octahedra	0.25	100	612	34
	CuO-G composite	0.06, 0.6	25, 60	700, 400	35
	CuO octahedra/3DGN	0.1	50	405	36
	porous CuO/Cu <sub>2</sub> O@CeO <sub>2</sub>	0.2	100	592.3	32
prepared by other routes	multilayer CuO@NiO hollow spheres	0.1	200	1061	7
	Hierarchical Cu nanosheets @ CuO nanorods	0.067	200	620	16
	core-shell CuO/PPy nanoleaves	0.2	45	760	18
	CuO micro-cog film	0.03	10	810	21

---

hollow-spherical CuO	0.067	55	543.9	22
CuO-CNT composite nanomicrospheres	0.067	25	500	19

---

Table S2. The resistances determined by EIS with cycling for HPCO electrode. Values were calculated with the above equivalent circuit model in Figure S8 (bottom).

Samples	$R_e$ (ohm)	$R_{SEI}$ (ohm)	$R_{ct}$ (ohm)
initial $0.1 \text{ A g}^{-1}$	2.203	15.69	0.09234
$4 \text{ A g}^{-1}$	3.201	7.573	0.01003
back $0.1 \text{ A g}^{-1}$	3.225	8.869	0.02972